Supplemental Figure 1

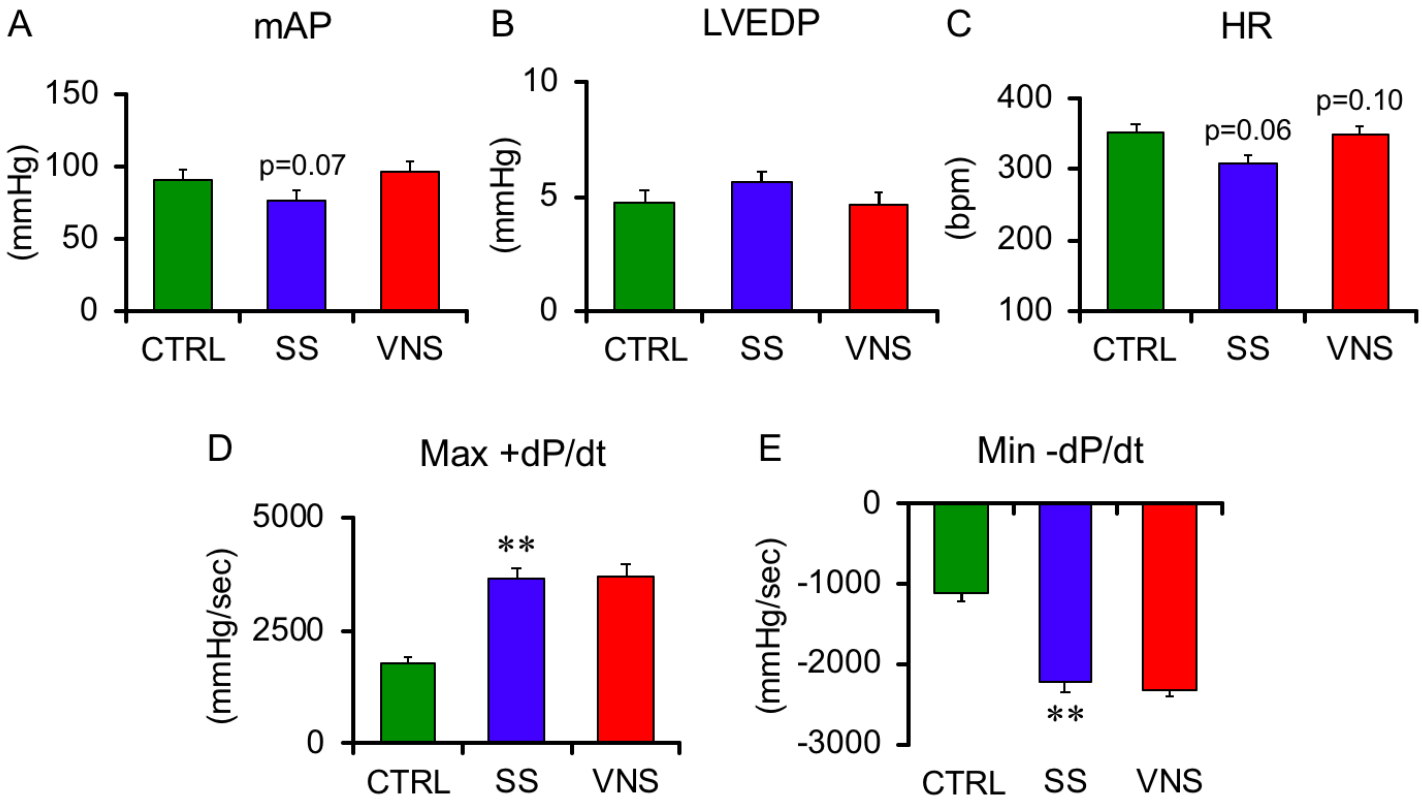

The effects of chronic vagal nerve stimulation (VNS) on hemodynamics in control (CTRL, n=5), sham stimulation (SS, n=6) and VNS (n=6) rats 5 weeks after SU5416 injection. There are no significant differences in mean arterial pressure (mAP), left ventricular end-diastolic pressure (LVEDP), or heart rate (HR) among 3 groups (A-C). Max +dP/dt (D) and Min –dP/dt (E) of RV are significantly higher in SS than in CTRL, while there are no significant differences between VNS and SS. Data are expressed as mean ± SEM. Differences were tested by one-way analysis of variance, followed by post-hoc Tukey-Kramer test.

**p < 0.01 vs. CTRL.

SUPPLEMENTAL MATERIALS:

Assessment of heart rate variability

Beat to beat (RR) intervals were obtained from 10-min telemetric ECG recording during daytime. The RR-interval time series were used to derive power spectral density (PSD, $msec^2/Hz$) by Fourier transform, plotting power in milliseconds squared per Hertz ($msec^2/Hz$) versus Hertz, for frequencies up to 2.0 Hz. The frequency range of 0.04–0.73 Hz was defined as low frequency (LF) and 0.73–2.0 Hz as high frequency (HF) (1).

Hemodynamic assessment and right ventricular hypertrophy

Hemodynamic data were recorded under general anesthesia with a mixture of urethane (250 mg/mL) + α-chloralose (40 mg/mL) and mechanical ventilation. Each signal is obtained at 1000 Hz using a 16-bit analog-to-digital converter (Power Lab 16/35, AD Instruments, Sydney, Australia) and stored in a dedicated laboratory computer system. LV end-diastolic pressure (LVEDP) and right ventricular (RV) end-diastolic pressure (RVEDP) were averaged for at least 10 sequential beats. Both Max +dP/dt and Min –dP/dt in RV pressure were calculated from the first time derivative of instantaneous RV pressure (2). Max +dP/dt was divided by RVEDP to normalize the preload effect. Pulmonary vascular resistance (PVR) was calculated as follow: PVR = (mean PAP – LVEDP)/CO.

Collection of lung and right heart samples for histological analysis

At the end of each hemodynamic study in protocol 1B, the lungs were inflated

with 10% formalin plus 0.5% agarose at 20 cm H_2O pressure, and fixed in 10% formalin overnight. The left and right lobes were blocked and paraffin embedded. All sections were cut at 5-μm. The right heart was also harvested and immediately fixed in buffered 10% paraformaldehyde, embedded in paraffin, and cut into 5-μm thick sections.

Luminal occlusive lesion of pulmonary arteries

Verhoeff van Gieson (EVG) staining was performed for morphometric analysis of pulmonary arteries. All small PAs (more than 100 vessels per cross-section of left lobes including the hilum, outer diameter < 100 μm) were evaluated. Vessels were assessed for occlusive neointimal lesions on EVG-stained slides and scored as: no evidence of neointimal formation (grade 0), partial luminal occlusion (< 50 %, grade 1), or severe-luminal occlusion (≥ 50 %, grade 2). PA occlusion rate was expressed as percentage for each grade. We assessed the vessels with outer diameter (OD) ≤ 50 μm and 50 < OD < 100 μm (3).

Macrophage migration of pulmonary arteries

Macrophages were detected by immunostaining using anti-CD68 antibody (1:50 dilution; MCA341B, Serotec). The number of CD68-positive cells were counted within a 100-μm diameter circle around the vessel (outer diameter, 30-70 μm) in 10 random fields at ×400 magnification (4).

Cell proliferation of pulmonary arteries

The number of proliferative cells was evaluated by anti-Ki67 antibody (1:400 dilution; RM-9106-S1, Thermo Scientific). Ki67positive cells were counted within a 100-

μm diameter circle around the vessel (outer diameter, 30-70 μm) in 10 random fields at ×400 magnification (4).

Apoptotic cells of pulmonary arteries

Apoptotic cells were labeled using a TdT-mediated dUTP-biotin nick end labeling (TUNEL) *in situ* apoptosis detection kit (MK500, Takara). TUNEL-positive cells in pulmonary arteries (outer diameter, 30-70 μm) were counted in 10 random fields at ×400 magnification (5).

Fibrosis of right ventricle

Masson Trichrome (MT) staining was performed on serial sections of the right ventricle. The percentage of fibrotic area was quantified on digitized images: blue-stained tissue area was expressed as a percentage of the total surface area of RV (6).

Capillary density of right ventricle

Capillary epithelium was detected by anti-CD34 antibody (1:100 dilution; LS-C150289, LS Bio). Capillary density was expressed as the number of capillaries per section area, measured in at least three randomly chosen areas per ventricle, where cardiomyocytes were transversally sectioned at ×400 magnification (7).

Apoptotic ratio of right ventricle

Apoptotic ratio was expressed as the number of TUNEL-positive myocytes divided by the total number of cardiomyocytes per field. Apoptosis was assessed in at least three randomly chosen areas per ventricle, where cardiomyocytes were transversally

sectioned at ×200 magnification (6).

Immunoblot analysis of the expression of eNOS and phospho-eNOS

In protocol 2, harvested lungs were frozen at -80°C and then homogenized in HEPES buffer. The protein concentration of the lysate was determined using a Coomassie protein assay kit (Pierce, Rockford, IL, USA) with bovine serum albumin as standard. Ten μg of protein was used to detect the expression of endothelial nitric oxide synthase (anti-eNOS antibody; 1:5,000; #9572, CST, Danvers, USA) and phosphorylated-eNOS (anti-phospho-eNOS; 1:2,000; #9571, CST, Danvers, USA) (8). The protein amount was normalized by the loading control, β-actin (anti-β-actin; 1:2,000; #E2710, CST, Danvers, USA).

RT-PCR analysis

In protocol 2, total RNA of lung tissue was extracted using the RNeasy Mini Kit (QIAGEN). The mRNA levels were determined by real-time PCR. For reverse transcription and amplification, we used the ReverTra Ace qPCR Kit (TOYOBO) and SYBR Premix Ex Taq (TaKaRa), respectively. The acquired fluorescence data were analyzed by ΔΔCt method, with *18s* as internal control.

PCR primers

Symbol	Sequence	
Il1b	Forward	5’-CCC TGA ACT CAA CTG TGA AAT AGC A-3’
	Reverse	5’-TTC CAA GCC CTT GAC TTG GG-3’
Il6	Forward	5’-ATT GTA TGA ACA GCG ATG ATG CAC-3’
	Reverse	5’-TCT GGA GTT CCG TTT CTA CCT GG-3’
Tnfa	Forward	5’-TCA GTT CCA TGG CCC AGA C-3’
	Reverse	5’-AGC AGT TAA GGC TGA GTT GTC TGA A-3’
Mcp1	Forward	5’-TGT GAG GCT CAT CTT TGC CAT C-3’
	Reverse	5’-CAC CTG CAT GGC CTG GTC TA-3’
Il10	Forward	5’-CAG ACC CAC ATG CTC CGA GA-3’
	Reverse	5’-CAA GGC TTG GCA ACC CAA GTA-3’
Alpha7nachr	Forward	5’-TGG TGA CAG TGA TTG TGC TGA GA-3’
	Reverse	5’-ACC ATG CAC ACC AGT TCA GGA G-3’
18s	Forward	5’-CCC TGA ACT CAA CTG TGA AAT AGC A-3’
	Reverse	5’-CCC AAG TCA AGG GCT TGG AA-3’

References in SUPPLEMENTAL MATERIAL:

1. Sanyal SN, Ono K. Derangement of autonomic nerve control in rat with right ventricular failure. Pathophysioly 2002;8:197–203.
2. GLEASON WL, BRAUNWALD E. Studies on the first derivative of the ventricular pressure pulse in man. J Clin Invest 1962;41:80–91.
3. Toba M, Alzoubi A, O'Neill KD, et al. Temporal hemodynamic and histological progression in Sugen5416/hypoxia/normoxia-exposed pulmonary arterial hypertensive rats. Am J Physiol Heart Circ Physiol 2014;306:H243–250.
4. Abe K, Shinoda M, Tanaka M, et al. Haemodynamic unloading reverses occlusive vascular lesions in severe pulmonary hypertension. Cardiovasc Res 2016;111:16–25.
5. Long L, Ormiston ML, Yang X, et al. Selective enhancement of endothelial BMPR-II with BMP9 reverses pulmonary arterial hypertension. Nat Med 2015;21:777–785.
6. Bogaard HJ, Mizuno S, Hussaini AA Al, et al. Suppression of histone deacetylases worsens right ventricular dysfunction after pulmonary artery banding in rats. Am J Respir Crit Care Med 2011;183:1402–1410.
7. De Man FS, Handoko ML, Van Ballegoij JJM, et al. Bisoprolol delays progression towards right heart failure in experimental pulmonary hypertension. Circ Heart Fail 2012;5:97–105.
8. Tanaka M, Abe K, Oka M, et al. Inhibition of nitric oxide synthase unmasks vigorous vasoconstriction in established pulmonary arterial hypertension. Physiol Rep 2017;5:e13537.